

Dynamical signature in spatial spin distributions of relativistic electrons

P Krekora, Q Su and R Grobe

Intense Laser Physics Theory Unit and Department of Physics, Illinois State University, Normal, IL 61790-4560, USA

Received 22 December 2000

Abstract

The time-dependent Dirac equation has been solved for an electron in external static electric, static magnetic and time-dependent electromagnetic fields. We give several examples of how the dynamics of the spin variables can couple to the relativistic orbital motion and investigate the time evolution of the spatial spin distribution as a function of the position for a relativistic quantum state.

1. Introduction

Spin is possibly the best known example of a quantum mechanical observable that does not have a trivial classical counterpart. Spin is, of course, of fundamental importance in labelling and characterizing atomic energies and associated eigenstates. The coupling of the spin variable to the position or the velocity (spin-orbit coupling) has mainly been investigated in the context of atomic structure. On the other hand, the famous Stern-Gerlach experiment is one of only a few examples in which the spin actually has a dynamical impact on the spatial motion. In this case non-relativistic field-spin coupling is due to the spatial inhomogeneity of the magnetic field. If the electron is non-relativistic, a homogeneous magnetic field does not couple the spin to the spatial variables and the spin performs a simple precession motion at the Larmor frequency. In this paper we will show how the dynamics of the spin in a homogeneous magnetic field can depend on the position and velocity of an electron in the relativistic regime.

Analytical solutions in the relativistic regime are very difficult to obtain due to the nonlinearity induced by relativity and one depends mostly on numerical solutions to the Dirac equation. Recently, using numerical wavefunction solutions to the one-dimensional-Dirac equation, the time dependence of the spin has been calculated for an electron ionizing in a strong laser field [1]. In this case the time evolution was described by the direct coupling of the spin to the electromagnetic field and not to the electron's position or its velocity. To the best of our knowledge, there are no studies that investigated how the dynamics of the spin variable can couple to the velocity or the position within a single quantum state. Is it possible to assign to a single quantum state a spin distribution as a function of space and time? Are there spatial regions in which the measurement of a certain spin value is more probable than at another location?

Here we have made a first attempt to investigate these problems. This work is part of an ongoing project to explore novel relativistic phenomena that do not have an immediate classical relativistic counterpart [2]. We do not investigate how the spin affects the orbital motion, but we focus our attention on the question of how the spin's dynamics depends on the orbital motion.

This paper is organized into three parts of increasing complexity. In section 2 we review how the Lorentz contraction of the spin for an electron accelerated in a static electric field can lead to a position-dependent spin distribution. In section 3 we study the spin of an electron in a static homogeneous magnetic field where the laser field is used to resonantly excite the electron into a high-speed orbit. In contrast to the first example, in this case the spin is coupled directly to the magnetic field, but for simplicity we will treat the orbital motion non-relativistically. Section 4 deals with the relativistic spin dynamics of cycloatoms [3]. We will discuss how a combination of the effects introduced in sections 2 and 3 will lead to a non-trivial dependence of the spin on the genuinely relativistic orbital motion.

In each of the three investigations we have compared our approximate analytical predictions based on classical mechanics with exact numerical wavefunction solutions to the full time-dependent Dirac equation [4],

$$i \frac{\partial}{\partial t} \Psi(\mathbf{r}, t) = \left[c \boldsymbol{\alpha} \left(\mathbf{p} + \frac{1}{c} \mathbf{A}(\mathbf{r}, t) \right) + \beta c^2 \right] \Psi(\mathbf{r}, t) \quad (1.1)$$

where $\boldsymbol{\alpha}$ and β are the 4×4 Dirac matrices, c is the speed of light ($c = 137.036$ in atomic units), $\mathbf{A}(\mathbf{r}, t)$ is the vector potential associated with the external field and $\Psi(\mathbf{r}, t) = (\Psi_1, \Psi_2, \Psi_3, \Psi_4)$ denotes the four-component Dirac spinor. The Dirac equation has been solved on a spacetime grid using a recently developed split-operator algorithm based on the fast Fourier transformation that is accurate up to the fifth order in time [5].

As the initial state in each of our calculations we have used

$$\Psi(\mathbf{r}, t = 0) = (2\pi \Delta x_0^2)^{-3/4} \exp[-(\mathbf{r}/\Delta x_0)^2/4] \Phi_{x,z}. \quad (1.2)$$

We used $\Phi_x = (1, 1, 0, 0)/\sqrt{2}$ and $\Phi_z = (1, 0, 0, 0)$ to represent initial spin states with averages $\langle S_x(t = 0) \rangle = \frac{1}{2}$ au and $\langle S_z(t = 0) \rangle = \frac{1}{2}$ au, respectively.

2. Relativistic orbits without field–spin coupling

In the first example, we will show how the relativistic Lorentz contraction of the spin due to large orbital speeds can lead to a position-dependent spin density. We illustrate this effect in its purest form without any other spin-coupling and choose the simplest possible case of an electron that is accelerated in a static electric field. This field is of strength E and it points towards the negative x -axis, such that $\mathbf{A}(\mathbf{r}, t) = cEt\mathbf{e}_x$.

In figure 1 we present five snapshots of the electron's spatial probability density along the x -axis defined by $P(x, t) = \iint dy dz \sum_{i=1}^4 |\Psi_i(\mathbf{r}, t)|^2$, where the summation extends over all four spinor components of the wavefunction. As the electron accelerates along the x -axis it spreads spatially until its speed approaches c . In that limit the spreading is relativistically suppressed and the wavepacket develops into a slightly asymmetric form [6].

In figure 1(b) we display the time dependence of the spin $\langle S_z(t) \rangle$ computed from the expectation value of the corresponding 4×4 spin matrix using the numerical wavefunction solution of the Dirac equation. The spin along the propagation axis $\langle S_x(t) \rangle$ is practically constant, whereas the spin perpendicular to the x -axis ($\langle S_z(t) \rangle$) decays as the electron's speed increases. This decay is associated with the Lorentz spin contraction which is different from the Lorentz length contraction in that the perpendicular component rather than the parallel

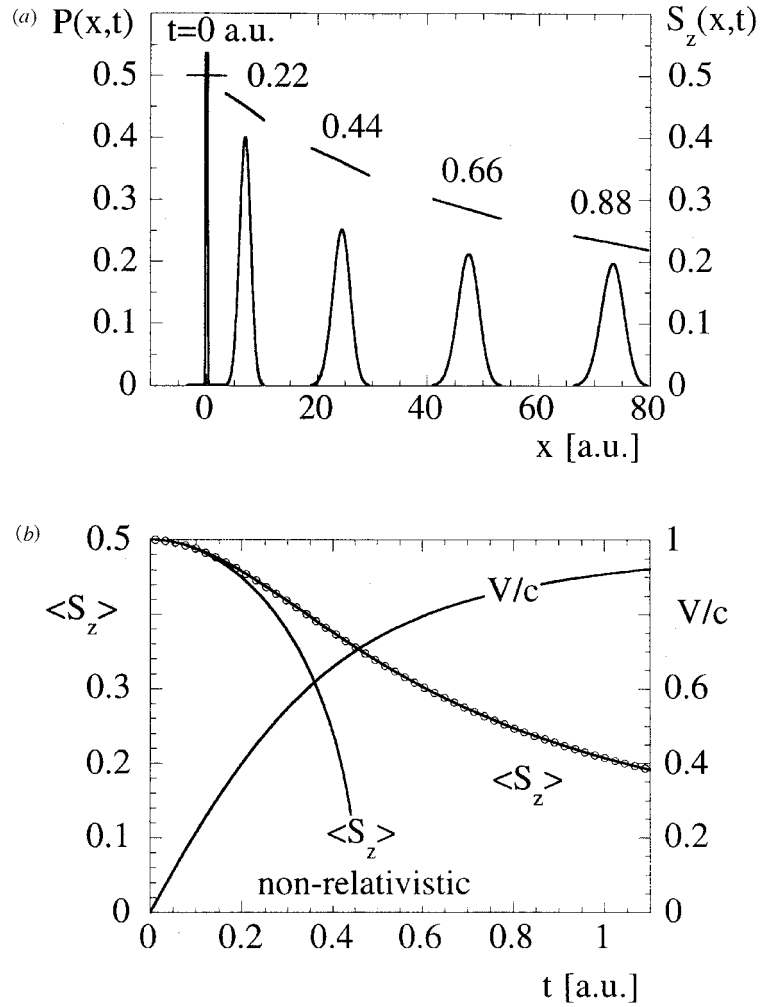


Figure 1. Electron wavepacket in a static electric field. (a) Snapshots of the spatial probability density taken at various times $t = 0, 0.22, 0.44, 0.66$ and 0.88 au. The disconnected lines are the spin-densities associated with each state. For graphical clarity the spin distributions are only displayed in those spatial areas in which the spatial probability distribution is larger than 10^{-3} . ($E = 300$ au, $\Delta x = 0.1$ au.) (b) The average value of the spin (in au) as a function of time. Superimposed by the circles are the predictions according to equation (2.7). The other curves are the predictions of the classical model based on a non-relativistic orbit. The calculation using a relativistic orbit is graphically indistinguishable from the quantum mechanical curve.

component is affected by the relativistic motion. The spin decay can be understood if we perform a Lorentz transformation into the electron's rest frame in which the spin remains constant if the negative energy components in the state are not significant. The spin, when observed from the laboratory frame (in which the Dirac equation is solved), appears to be contracted by the Lorentz-gamma factor,

$$\langle \mathcal{S}(V) \rangle = [1 - (V_{\perp}/c)^2]^{1/2} \langle \mathcal{S}(V = 0) \rangle \quad (2.1)$$

where V_{\perp} denotes the velocity component perpendicular to the spin vector \mathcal{S} [7]. In figure 1(b) we have superimposed on the exact curve the predictions of this formula (circles), where we

have used the corresponding classical relativistic solution for a point particle

$$V_x(t) = [V_{0x}/(1 - V_{0x}^2/c^2)^{1/2} + Et]\{1 + [V_{0x}/(1 - V_{0x}^2/c^2)^{1/2} + Et]^2/c^2\}^{-1/2} \quad (2.2)$$

which approximates the speed of the centre of mass $\langle V_x \rangle$ quite well for electron wavepackets with small velocity dispersion. The agreement with the quantum computation is excellent. To demonstrate the importance of relativity with respect to the orbital motion, we also show a graph for the spin that was based on the non-relativistic speed, $V_x(t) = V_{0x} + Et$, and the agreement is clearly only good at early times, $t < 0.2$ au, for which $V_x/c \ll 1$. For the parameters used in the calculation, the average velocity was $\langle V_x(t) \rangle/c = 0.92$ after a time of 1.1 au.

Next, we will address the question of how the spin is distributed along the wavepacket. In figure 1(b) the average value of the spin was calculated from the corresponding 4×4 operator matrix S_z , in the standard Pauli representation via

$$\begin{aligned} \langle S_z(t) \rangle &= \langle \Psi(\mathbf{r}, t) | S_z | \Psi(\mathbf{r}, t) \rangle \\ &= \iiint dx dy dz [|\Psi_1(\mathbf{r}, t)|^2 - |\Psi_2(\mathbf{r}, t)|^2 + |\Psi_3(\mathbf{r}, t)|^2 - |\Psi_4(\mathbf{r}, t)|^2]/2 \end{aligned} \quad (2.3)$$

which suggests that the integrand could be interpreted in terms of classical statistical mechanics as the product of a ‘position-dependent spin variable’ $S_z(\mathbf{r}, t)$ and a corresponding probability distribution. We define here a spatial spin distribution function by the ratio [8]:

$$S_z(\mathbf{r}, t) \equiv \frac{1}{2} \frac{|\Psi_1(\mathbf{r}, t)|^2 - |\Psi_2(\mathbf{r}, t)|^2 + |\Psi_3(\mathbf{r}, t)|^2 - |\Psi_4(\mathbf{r}, t)|^2}{|\Psi_1(\mathbf{r}, t)|^2 + |\Psi_2(\mathbf{r}, t)|^2 + |\Psi_3(\mathbf{r}, t)|^2 + |\Psi_4(\mathbf{r}, t)|^2}. \quad (2.4)$$

Obviously, for other spin directions it can be defined similarly as $S(\mathbf{r}, t) \equiv \Psi^\dagger(\mathbf{r}, t) \mathbf{S} \Psi(\mathbf{r}, t) / \Psi^\dagger(\mathbf{r}, t) \Psi(\mathbf{r}, t)$. We will demonstrate below that this quantity matches well the corresponding spatial spin distribution for a classical ensemble of spins. In other words, one could be tempted to interpret $S(\mathbf{r}, t)$ as the average value of the spin one would measure if the electron were detected at time t at location \mathbf{r} . Please note that the reference to the word ‘average’ is used in a quantum statistical sense; any individual spin measurement, of course, leads to $\pm \frac{1}{2}$ au. From this definition it follows that $\langle S_z(t) \rangle = \langle \Psi(\mathbf{r}, t) | S_z | \Psi(\mathbf{r}, t) \rangle = \iiint dx dy dz S_z(\mathbf{r}, t) P(\mathbf{r}, t)$, where $P(\mathbf{r}, t) \equiv \Psi^\dagger(\mathbf{r}, t) \Psi(\mathbf{r}, t)$ is the usual spatial probability density, given by the sum of the four squared spinor components of the wavefunction.

On top of the state in figure 1(a) we display the five spin distributions $S_z(x, t)$ computed from the wavepackets. The corresponding distribution $S_x(x, t)$ along the direction of propagation remains constant spatially as well as temporally, $S_x(x, t) = \frac{1}{2}$ au. Initially, the state was in a spin eigenstate, and remains so throughout the time evolution. In other words, the spin operator S_x commutes with the Dirac Hamiltonian in one spatial direction, and the momentum eigenstates with velocities along the x -direction are also spin S_x eigenstates. For a direction perpendicular to the x -direction, the situation is different; the spin is not a good quantum number for a wavepacket and $S_z(x, t)$ decreases as a function of time and space. It is quite interesting to note that in addition to the overall lowered spin value from snapshot to snapshot, the spin distribution is non-uniform. The spins associated with the front edge of the accelerated wavepacket are relatively smaller, reflecting the fact that the larger velocity components of the wavepacket have travelled to the right-hand edge of the quantum state. One can actually view the spin distribution $S_z(x, t)$ as a spatially resolved ‘speedometer’ for the quantum mechanical state in this case.

To justify this statement quantitatively, we have calculated a ‘classical’ spin distribution from the classical Liouville phase-space density [9]:

$$S_z^{\text{class}}(\mathbf{r}, t) = \int d\mathbf{p} \frac{1}{2} \sqrt{1 - (\mathbf{V}_\perp(\mathbf{p})/c)^2} \rho(\mathbf{r}, \mathbf{p}, t). \quad (2.5)$$

It can be obtained from the initial density $\rho(\mathbf{r}, \mathbf{p}, t = 0) \equiv \rho_0(\mathbf{r}, \mathbf{p})$ via

$$\rho(\mathbf{r}, \mathbf{p}, t) = \iint d\mathbf{r}_0 d\mathbf{p}_0 \rho_0(\mathbf{r}_0, \mathbf{p}_0) \delta[\mathbf{r} - \mathbf{r}(\mathbf{r}_0, \mathbf{p}_0, t)] \delta[\mathbf{p} - \mathbf{p}(\mathbf{r}_0, \mathbf{p}_0, t)] \quad (2.6)$$

where $\mathbf{r}(\mathbf{r}_0, \mathbf{p}_0, t) \equiv \mathbf{r}_0 + \mathbf{a}(\mathbf{p}_0, t)$ and $\mathbf{p}(\mathbf{r}_0, \mathbf{p}_0, t)$ denote the corresponding single-trajectory solutions to the relativistic Newton equations with the initial values \mathbf{r}_0 and \mathbf{p}_0 . Performing the integration over \mathbf{r}_0 and \mathbf{p} we find the simple expression:

$$S_z^{\text{class}}(\mathbf{r}, t) = \int d\mathbf{p}_0 \frac{1}{2} \sqrt{1 - V_{\perp}^2[\mathbf{p}(\mathbf{p}_0, t)]/c^2} \rho_0(\mathbf{r} - \mathbf{a}(\mathbf{p}_0, t), \mathbf{p}_0). \quad (2.7)$$

As an initial phase space density we have used

$$\rho_0(\mathbf{r}, \mathbf{p}) = (1/\pi^3) \exp[-(\mathbf{r}/\Delta x)^2/2] \exp[-2(\mathbf{p}\Delta x)^2]$$

which has the same (symmetrized) average values as the quantum mechanical expectation values calculated from the Dirac state equation (1.2). We have superimposed in figure 1(b) the classical spin distribution $S_z^{\text{class}}(x, t) = \iint dy dz S_z^{\text{class}}(\mathbf{r}, t)$ according to equations (2.7) and (2.4). It is practically indistinguishable from the exact Dirac spin distribution. This perfect agreement demonstrates that some kinetic aspects of the spin dynamics can be quite well approximated by concepts of classical (relativistic) mechanics.

3. Non-relativistic orbits with direct field–spin coupling

Let us now investigate the Lorentz contraction for a more complicated case in which the spin variables are coupled directly to a static homogeneous magnetic field along the z -direction. In order to bring the electron to a high speed orbit [10] we have used an additional time-dependent electric field, $\mathbf{E}(t) = E \sin(\omega_L t) \mathbf{e}_x$, whose frequency ω_L was chosen to be close to the cyclotron frequency $\Omega = B/c$ associated with the magnetic field of $\mathbf{B} = B\mathbf{e}_z$. To remain focused on the effect of the Lorentz spin contraction, we exclude here for better clarity any relativistic effects on the orbital motion. In section 4 we will demonstrate how the relativistic treatment of the orbital motion will complicate the spin dynamics. The vector potential in this case is given by $\mathbf{A}(\mathbf{r}, t) = -cE \sin(\omega_L t)/\omega_L \mathbf{e}_x - \frac{1}{2}c\Omega y \mathbf{e}_x + \frac{1}{2}c\Omega x \mathbf{e}_y$. In the absence of any relativistic spin–velocity coupling, the Dirac Hamiltonian has a non-relativistic limit [11] of the form $H = [\mathbf{p} + \mathbf{A}(\mathbf{r}, t)/c]^2/2 - cS_z\Omega$, which leads to simple Larmor precession motion according to $\langle S_x(t) \rangle = \cos(\Omega t)/2$ and $\langle S_z(t) \rangle = \frac{1}{2}$ for our two initial states.

Let us first discuss the Lorentz spin contraction for wavepackets with a large initial spatial width Δx . In this case the corresponding distribution of velocities is relatively narrow ($\Delta V = 1/(2\Delta x)$) and we can approximate the state by a single (time-dependent) velocity. This velocity and the positions are identical to those of the corresponding classical non-relativistic trajectory solution to a system with $H = \frac{1}{2}(\mathbf{p} + \mathbf{A}(\mathbf{r}, t)/c)^2$:

$$x(t) = x_0 + V_{0x}/\Omega \sin(\Omega t) + V_{0y}/\Omega [\cos(\Omega t) - 1] + A[\cos(\Omega t) - \cos(\omega_L t)] \quad (3.1a)$$

$$y(t) = y_0 + V_{0y}/\Omega \sin(\Omega t) - V_{0x}/\Omega [\cos(\Omega t) - 1] + A[\sin(\Omega t) - \Omega/\omega_L \sin(\omega_L t)] \quad (3.1b)$$

$$V_x(t) = V_{0x} \cos(\Omega t) - V_{0y} \sin(\Omega t) - A[\Omega \sin(\Omega t) - \omega_L \sin(\omega_L t)] \quad (3.1c)$$

$$V_y(t) = V_{0y} \cos(\Omega t) + V_{0x} \sin(\Omega t) + A\Omega[\cos(\Omega t) - \cos(\omega_L t)] \quad (3.1d)$$

with the resonant amplitude $A = E/[(\omega_L^2 - \Omega^2)]$. Unless the two frequencies are commensurate, the motion is not periodic and corresponds to a spiral-type trajectory. As shown above, the Lorentz contraction depends only on the velocity component that is perpendicular

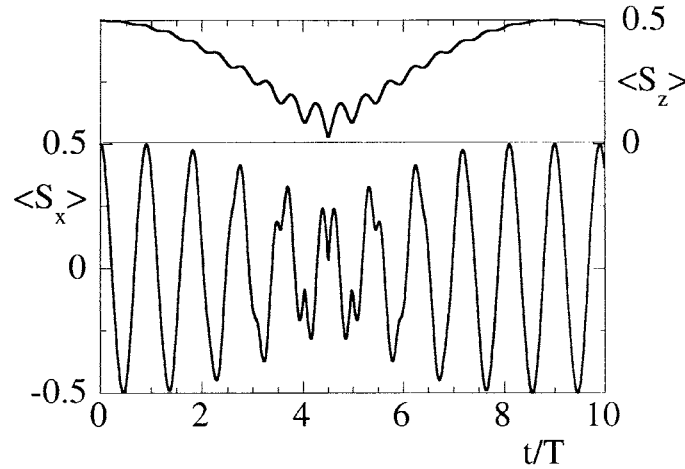


Figure 2. Electron wavepacket in a static magnetic field and a laser field. The expectation value of the spin (in au) perpendicular and parallel to the motion as a function of time (in units of the laser period $T = 2\pi/\omega_L$). ($V_{0x} = V_{0y} = 0$ au, $x_0 = y_0 = 0$, $\Omega = 100$ au, $E = 1300$ au, $\omega_L = 90$ au).

to the spin, e.g. $\langle S_x(t) \rangle$ depends only on V_y and its evolution would be modulated by a time-dependent Lorentz contraction according to

$$\langle S_x(t) \rangle = \frac{1}{2} \cos(\Omega t) \sqrt{1 - (V_y(t)/c)^2} \quad (3.2a)$$

$$\langle S_z(t) \rangle = \frac{1}{2} \sqrt{1 - (V_x(t)/c)^2 - (V_y(t)/c)^2}. \quad (3.2b)$$

In figure 2 we show that the Lorentz contraction can affect the precession motion of the spins $\langle S_x(t) \rangle$ and $\langle S_z(t) \rangle$. The amount of Lorentz contraction depends on the parameters E , Ω , and ω_L , leading to a non-periodic time evolution of the spin. The top line displays the average value of the spin $\langle S_z \rangle$ which approximately follows the velocity.

Next we will analyse the corresponding spatial spin distributions. Non-uniform spatial distributions are most pronounced for initially narrow states, associated with a larger spread in velocities. In addition to the Larmor precession, the spins are also Lorentz-contracted due to the corresponding velocities. As the amount of this contraction for S_x and S_z depends directly on V_y and $V = |\mathbf{V}|$, respectively, we need to analyse the velocity distribution within the wavepacket. Spatial areas of the same velocities will have the same amount of spin contraction. To model an initially narrow wavepacket we have assumed $x_0 = y_0 = 0$ and eliminated the initial velocities V_{0x} and V_{0y} from equations (3.1) to obtain the velocities as a function of the position for a given time t

$$V_x(\mathbf{r}, t) = \frac{\Omega}{2} \left[\frac{\sin \Omega t}{1 - \cos \Omega t} x - y \right] + f(t) \quad (3.3a)$$

$$V_y(\mathbf{r}, t) = \frac{\Omega}{2} \left[x + \frac{\sin \Omega t}{1 - \cos \Omega t} y \right] + g(t) \quad (3.3b)$$

where the two functions $f(t)$ and $g(t)$ are independent of the position. Using these position-dependent velocities one can easily see that the lines of equal velocity V_y are straight lines with time-dependent slopes. The contour lines of equal total velocity V are concentric circles with a time-dependent centre.

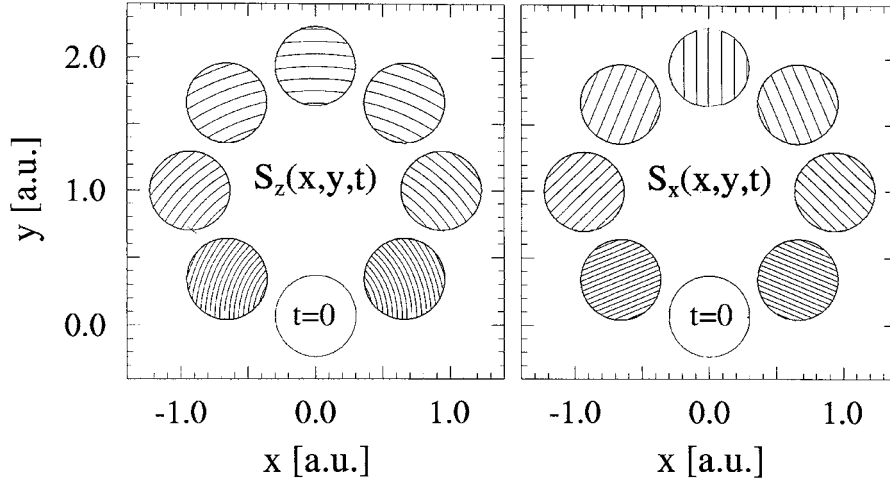


Figure 3. Electron wavepacket in a static magnetic field. Snapshots of the contour lines of the spatial spin distribution. The circles are centred around the actual orbit as described by equations (3.1). ($V_{0x} = 100$ au, $V_{0y} = 0$, $x_0 = y_0 = 0$, $\Omega = 100$ au, $E = 0$, the contour levels differ by a velocity of 5 au).

In figure 3 we present the velocity contour lines for the special case of $E = 0$ for which $f(t) = g(t) = 0$ and an initial state with velocity $\mathbf{V}_0 = (100, 0, 0)$ au. To better guide the eye we have shown the contours only within circles, whose centres follow the (counterclockwise rotating) orbit described in equations (3.1a) and (3.1b) [12]. The bottom circle reflects the location of the initial state. The left-hand figure shows the contour lines of V at every eighth of the cyclotron period $2\pi/\Omega$. These lines are, of course, identical to the iso-spin lines for the spin distribution $S_z^{\text{class}}(x, y, t)$. At early times, the contour lines are more narrowly spaced; this reflects the fact that the different velocity contributions in the state require some time to drift apart. After half the cyclotron period we have the spatially widest velocity distribution as only velocities close to 100 au fit inside the ring whose centre is characterized by the speed $V = 100$ au. In each circle the contour lines with the largest radius correspond to the largest velocity (largest spin-contraction). This velocity radius R is related to the velocities according to $R = V\sqrt{2(1 - \cos\Omega t)}/\Omega$. The maximum radius (associated with time $\frac{1}{2}2\pi/\Omega$) amounts to $R = 2V/\Omega$, which is exactly twice the radius of the corresponding gyro-orbit associated with speed V .

The right-hand frame in figure 3 shows the iso-velocity lines for V_y . These correspond to the contour lines for the spin distribution $S_x^{\text{class}}(x, y, t)$ when multiplied with the Larmor-precession factor $\frac{1}{2}\cos(\Omega t)$. In contrast to S_z the contour lines are straight lines with a time-dependent slope of $-[1 - \cos(\Omega t)]/\sin(\Omega t)$.

It is interesting to note that in the absence of the laser field, $E = 0$, the spin $S_y(t)$ and the velocity $V_y(t)$ are perfectly ‘in phase’. In other words, the scalar product $\mathbf{S}(t) \cdot \mathbf{V}(t)$ is time independent as one can easily derive from the corresponding equations of motion. There are two interesting special cases. If we start with $\mathbf{S}(t = 0) = (\frac{1}{2}, 0, 0)$ au and $\mathbf{V}(t = 0) = (V_{0x}, 0, 0)$, the spin direction remains parallel to the rotating velocity vector and there is no Lorentz contraction at all with respect to the length of the spin vector. On the other hand, if we start with $\mathbf{S}(t = 0) = (0, \frac{1}{2}, 0)$ au and $\mathbf{V}(t = 0) = (V_{0x}, 0, 0)$, the spin direction remains perpendicular to the rotating velocity vector and the Lorentz contraction is constant. For the following discussion it is also important to note that the spin contraction,

though position dependent, only attenuates the spin and it is not possible to find locations within the wavepacket where the spin components take different signs.

4. Relativistic orbits with direct field–spin coupling

Let us now discuss the most complicated case for which the dynamics of the spin is governed by a velocity-dependent cyclotron (Larmor) frequency and the Lorentz contraction, which is a function of the orbital motion which itself is genuinely relativistic. The vector potential for this case is the same as in the previous section. There exist no analytical solutions for the relativistic orbit since the nonlinearity induced by the relativistic resonance makes the system non-integrable and even excites chaotic orbits [13]. Previous works [3, 10, 14] have shown that the spatial evolution of the wavepacket is characterized by the formation of ring-like probability distributions that rotate around the origin with the period of the laser [15].

The corresponding classical spatial probability distribution evolves similarly to the quantum Dirac state [16]. At early times the wavepacket follows a spiral-type orbit around the origin, but as the laser accelerates the particles up to relativistic speeds, the wavepacket becomes elongated with one end close to the origin. As the front end grows the packet evolves into a rotating ‘banana’ shape which then closes to a full circle.

The formation of these relativistic rings (called cycloatoms) can be crudely mimicked in terms of a dephasing model using a spatial distribution of quasiparticles, each of which performs a spiral-type orbit around the origin with a slightly different Larmor frequency [16]. By replacing the Larmor frequency Ω in the non-relativistic single-orbit trajectories (equations (3.1)) by one that varies slightly with the initial velocity, one models in a very crude way the fact that orbits with different initial velocities will experience different relativistic mass-shifts when accelerated close to c . For the regime of our numerical parameters ($\omega_L < \Omega$) the entire distribution rotates counterclockwise, whereas the tail grows in the clockwise direction relative to a coordinate frame that rotates with the laser frequency.

Let us now analyse the time evolution of the corresponding spin distribution for $S_z(\mathbf{r}, t)$ (magnetic field direction). For graphical clarity we show in figure 4 the spin distribution only for those spatial regions for which the probability density $\Psi^\dagger(\mathbf{r}, t)\Psi(\mathbf{r}, t)$ exceeds 6×10^{-6} . At early times, the packet is non-relativistic and we see the concentric ring-like contour lines reminiscent of those of the non-relativistic orbits explained in section 3 and displayed in figure 3. To better guide the eye, we have included in the figure an (arbitrary, broken) circle with the centre around the origin. The region around the origin has the smallest velocity contributions and therefore the smallest amount of Lorentz contraction. It is quite remarkable that even at later times ($t > 0.4$ au), when the tail end begins to curve inward towards the origin, the spin contour lines in the front edge of the growing tail still follow approximately the simple concentric circles. At later times when the tail end has closed the distribution to a full circle at time $t = 0.6$ au, the front tail again contains very small velocity contributions. This increase and decrease of the Lorentz contraction associated with different spatial parts of the distribution can be directly associated with outward- (accelerating) and inward-going (decelerating) spiral orbits associated with the classical dephasing model. As a result the spin distribution $S_z(\mathbf{r}, t)$ seems to depend mainly on the specific position and not so much on time.

The spin distribution $S_x(\mathbf{r}, t)$ at a given time t is the result of three independent relativistic effects. The first one is the Lorentz contraction, which restricts the maximum spin value; it depends only on the instantaneous velocity in the y -direction V_y . The second effect is due to the relativistic mass-shift, effectively leading to a velocity-dependent Larmor frequency; this effect is cumulative in the sense that the entire history of different Larmor frequencies

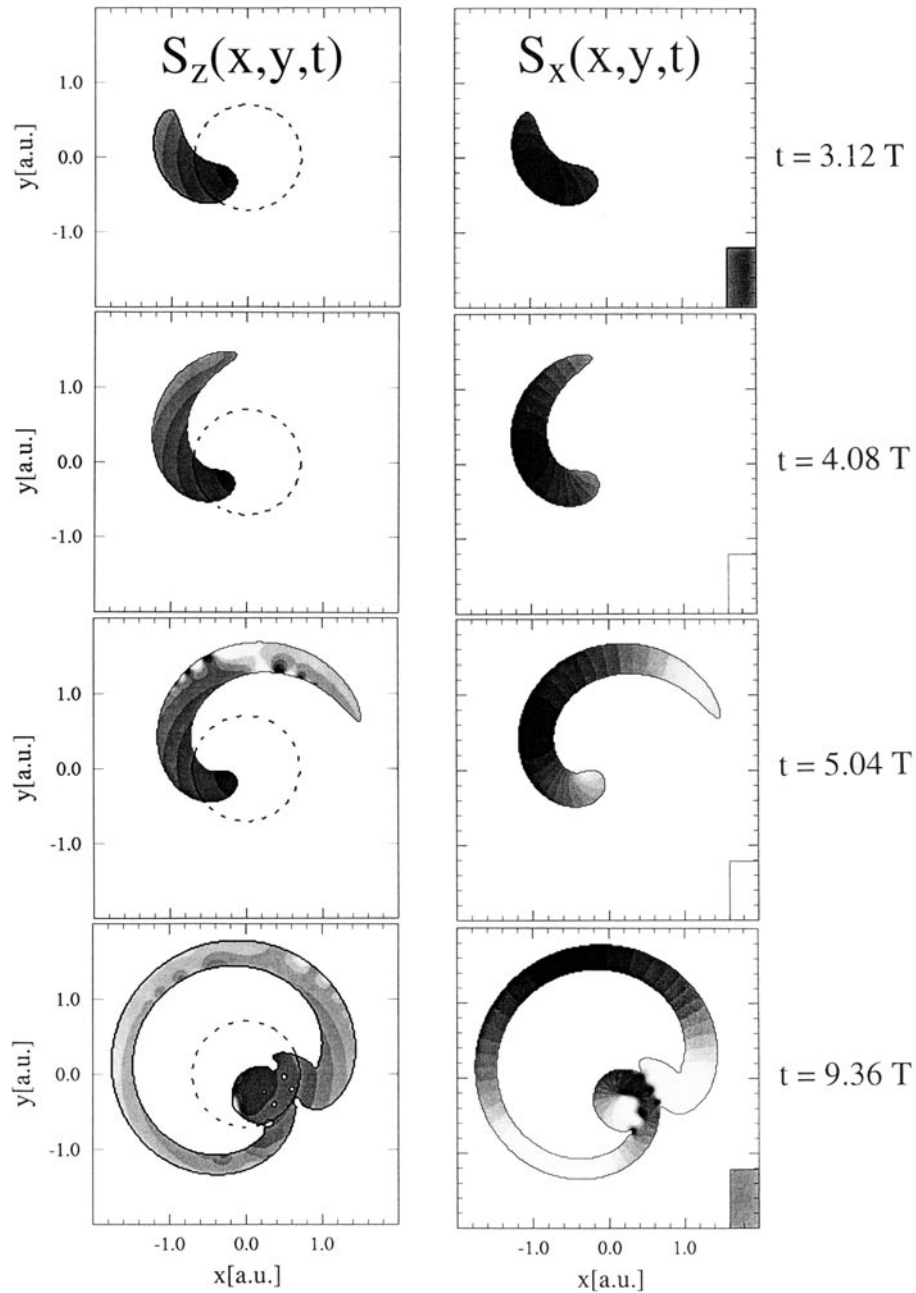


Figure 4. Snapshots of the spin distribution in relativistic cycloatoms at various times. The circle in the left-hand figures is arbitrary and added to guide the eye. ($V_{0x} = V_{0y} = 0$ au, $x_0 = y_0 = 0$, $\Omega = 96$ au, $E = 800$ au, $\omega_L = 80$ au).

contributes to the phase and the amplitude of the local spin value. A third effect is the well known Thomas precession [17], whose frequency for a uniformly accelerated system is given by $\omega_T = (\gamma - 1)\mathbf{a} \times \mathbf{V}/V^2$. Approximating $|\mathbf{a}|$ with $V\Omega$ and assuming an average value of

$V = c/4$ for the speed, the Thomas precession frequency $|(\gamma - 1)\Omega|$ would amount to $\Omega/31.5$, which is much smaller than the cyclotron frequency and corresponds for our parameters to a time even longer than the total duration of the interaction. As the final state is the result of these cumulative and non-cumulative effects, we discuss the impact of these effects step by step as the electron becomes relativistic.

In the right-hand frame of figure 4 we display the corresponding spin distribution S_x for a state initially with $\langle S_x(\mathbf{r}, t = 0) \rangle = \frac{1}{2}$ au. To better focus on the impact of relativity on the Larmor precession, we have indicated in the lower right-hand box the value of a function $\frac{1}{2} \cos(\Omega t)$ associated with a (spatially constant, but time-dependent) spin density of a wavepacket for which the spin is (artificially) decoupled from the orbital motion for each frame. In contrast to $S_z(\mathbf{r}, t)$ the spin contour lines for $S_x(\mathbf{r}, t)$ are not concentric circles. If the spin were only affected by the Lorentz effect, we would expect parallel lines as discussed in figure 3. However, in addition to this effect, the faster contributions in the leading tail experience a smaller effective Larmor frequency. As a result, the spin value lags behind the (spin-orbital decoupled) value of $\frac{1}{2} \cos(\Omega t)$. This effect curves the otherwise parallel contour lines. The snapshot at time $t = 4.08 T$ nicely illustrates both effects. Here $T = 2\pi/\omega_L$ is the laser period. The distributions at the centre and the tail end are out of phase but they have the same spin value. As the spins get out of phase in a continuous manner along the distribution, one could expect somewhere a maximum spin value of $\frac{1}{2}$ au. However, in this case the maximum value is associated with the leftmost part of the distribution ($(x, y) \approx (-1, 0)$ au) where the velocity V_y is largest. As a result the Lorentz contraction forbids the maximum value of $\frac{1}{2}$ in this region. A similar effect can be observed at later times $t = 9.36T$ when the spins of the front end and those close to the origin are completely out of phase. Here the maximum spin value $\frac{1}{2}$ au is taken at the uppermost part of the distribution where the Lorentz contraction is negligible ($V_y \approx 0$). We note that the contour lines recorded at the largest time $t = 9.36T$ are along straight lines; all of which seem to originate at various locations close to the origin.

Finally, we should mention that the product of the velocity and the spin operator $c\boldsymbol{\alpha} \cdot \mathbf{S}$ is nearly constant. The distribution $\Psi^\dagger c\boldsymbol{\alpha} \cdot \mathbf{S} / \Psi^\dagger \Psi$ depends neither on time nor on the position as the electron is accelerated. On the other hand, we found that the invariant operator $c\boldsymbol{\alpha} \cdot \mathbf{S}$ is not very helpful in interpreting our spin data, as the product of both individual distributions, $\Psi^\dagger c\boldsymbol{\alpha} \Psi \cdot \Psi^\dagger \mathbf{S} \Psi / [\Psi^\dagger \Psi]^2$ depends strongly on time and space, indicating that the strong correlation between $c\boldsymbol{\alpha}$ and \mathbf{S} does not permit a factorization of the expectation value.

Acknowledgments

We acknowledge help with the graphics by R E Wagner and P J Peverly. This work has been supported by the NSF under grant PHY-9970490. We also acknowledge support from the Research Corporation for Cottrell Science Awards and ISU for URGs. The numerical work has been performed at NCSA.

References

- [1] Rathe U W, Keltel C H, Protopapas M and Knight P L 1997 *J. Phys. B: At. Mol. Opt. Phys.* **30** L531
- [2] Su Q and Grobe R 2000 *Multiphoton Processes* ed L F DiMauro, R R Freeman and K C Kulander (Melville, NY: AIP) p 655
- [3] IP 2000 *Science News* **157** 287
Wagner R E, Su Q and Grobe R 2000 *Phys. Rev. Lett.* **84** 3282
- [4] Thaller B 1992 *The Dirac Equation* (Berlin: Springer)
- [5] Braun J W, Su Q and Grobe R 1999 *Phys. Rev. A* **59** 604

- For alternative algorithms, see, e.g. Rathe U W, Sanders P and Knight P L 1999 *Parallel Comput.* **25** 525
Wells J C, Umar A S, Oberacker V E, Bottcher C, Strayer M R, Wu L S, Drake J and Flanery R 1993 *Int. J. Mod. Phys. C* **4** 459
- [6] For relativistic suppression of wavepacket spreading, see, Su Q, Smetanko B A and Grobe R 1998 *Laser Phys.* **8** 93
Su Q, Smetanko B A and Grobe R 1998 *Opt. Express* **2** 277
- [7] For a review on Lorentz transformations of 4×4 spin matrices, see, e.g., Bjorken J D and Drell S D 1964 *Relativistic Quantum Mechanics* (New York: McGraw-Hill)
Kessler J 1985 *Polarized Electrons* 2nd edn (Berlin: Springer)
- [8] For work on the spin-Wigner function, see, e.g., Bialynicki-Birula I, Gornicki P and Rafelski J 1991 *Phys. Rev. D* **44** 1825
Shin G R, Bialynicki-Birula I and Rafelski J 1992 *Phys. Rev. D* **46** 645
- [9] Goldstein H 1980 *Classical Mechanics* 2nd edn (Reading, MA: Addison-Wesley)
- [10] Peverly P J, Wagner R E, Su Q and Grobe R 2000 *Laser Phys.* **10** 303
Su Q, Wagner R E, Peverly P J and Grobe R 2000 *Frontiers of Laser Physics and Quantum Optics* ed Z Xu, S Xie, S-Y Zhu and M O Scully (Berlin: Springer) p 17
- [11] See, e.g., Schiff L I 1968 *Quantum Mechanics* (New York: McGraw-Hill) ch 13
- [12] For the time evolution of the spatial width, see, Csesznegi J C, Rutherford G H, Su Q and Grobe R 1999 *Laser Phys.* **6** 41
- [13] Kim J H and Lee H W 1995 *Phys. Rev. E* **52** 473
Kim J H and Lee H W 1996 *Phys. Rev. E* **54** 3461
Lee S W, Kim J H and Lee H W 1997 *Phys. Rev. E* **56** 4090
- [14] Wagner R E, Su Q and Grobe R 1999 *Phys. Rev. A* **60** 3233
- [15] For movies of cycloatoms, see 2000 *Phys. Rev. Focus* **5** 15 <http://focus.aps.org/v5/st15.html> story
- [16] Wagner R E, Peverly P J, Su Q and Grobe R 2000 *Phys. Rev. A* **61** 35402
Krekora P, Wagner R E, Su Q and Grobe R 2001 *Phys. Rev. A* **63** 25404
- [17] Thomas L T 1927 *Phil. Mag.* **3** 1
Jackson J D 1999 *Classical Electrodynamics* (New York: Wiley)